



TECHNICAL ARTICLE

Influences of Directions and Magnitudes of Static Electrical Field on Microstructure and Mechanical Properties for Al–Si Eutectic Alloy

Semih Birinci, Sercan Basit, and Necmettin Maraşlı

Submitted: 10 June 2021 / Revised: 6 December 2021 / Accepted: 7 December 2021 / Published online: 11 January 2022

The aim of this article was to investigate the influences of directions and magnitudes of static electrical field (E) on eutectic spacings (λ), Brinell hardness (HB) and ultimate tensile strength (σ_{UTS}), yield strength (YS) and % elongation (%El) in the Al–12.6 wt.% Si alloy. For this purpose, the Al–12.6 wt.% Si molten alloy was solidified with different directions and magnitudes of E . Directions of E were chosen to be parallel (E_+) and antiparallel (E_-) to the solid–liquid (S–L) growth direction, and the magnitudes of E were in the range of 14.1–17.9 kV cm⁻¹. The E_+ and E_- provided an increment or decrement in the atomic mass flux of liquid Al atoms at S–L interface during the solidification. Thus, the value of λ increased as 100% and the values of HB and σ_{UTS} decreased as 6.3 and 6.2%, respectively, with increasing the E_+ . But the λ value decreased as 34% and the values of HB and σ_{UTS} are increased as 8.5 and 5.6%, respectively, with increasing E_- . The dependence of λ , HB and σ_{UTS} on the E_+ and E_- was determined by regression analysis.

Keywords Al–Si alloy, hardness, microstructure, solidification under electric field, ultimate tensile strength

1. Introduction

Aluminum is an ideal material to produce the housing and industrial materials, and they should possess both good castability and excellent mechanical properties. Die casting is the most common processing technology to produce Al-based alloys with thin-walled structures in industrial production. Pure aluminum has relatively poor mechanical properties, and thus, alloying is effective to enhance the mechanical properties of pure aluminum.

The Al–Si eutectic alloy is the mostly used as aluminum cast alloys in the transportation industry with their strong corrosion behavior, high ratio of strength to weight and castability. The melting conditions, temperature gradient, solidification rate, composition of the alloy and heat treatment that can be applied during and after casting are considered as the main control parameters to obtain the desired microstructure and mechanical properties of aluminum alloys (Ref 1-5).

Recently, the researchers have found new external solidification control parameters which are the semi-solid compaction,

agitation, ultrasonic vibration, selective laser melting, alternative current, direct current and DC voltage. They have concluded that the desired mechanical properties of alloys might be obtained by controlling these parameters during the solidification of alloy. In addition to these, there are extra cost-effective processes such as grain refinement and heat treatment to improve the mechanical properties of alloys (Ref 6, 7).

Vibration, compression and semi-solid shaping progresses are commonly preferred to break the secondary dendrite arms and change the morphology of Si during the solidification in the Al–Si eutectic alloy. The strength property of the material was improved by producing small secondary dendrite arm spacings (SDAS) and the changing the morphology of the Si (Ref 2, 8-12).

Alternative current, direct current and magnetic field as a new alternative external control parameters have been extensively applied into the molten alloys, and their effects on the microstructure and mechanical properties of the alloys were clearly observed (Ref 12-20). In addition, the electrical pulse effects on the distribution of the elements in the electro pulsing alloy (Ref 14) are determined. The molten Bi–Mn eutectic alloy was solidified with the alternating current, static electric field and magnetic field (Ref 15). Manuwong et al. (Ref 16) have concluded that the externally applied electro pulsing is more effective a control parameter than the magnetic flux and Lorentz force parameters in magnetic refinement.

Zhang et al. (Ref 17) have investigated the distribution of electric currents on the grain size of solidified Al–Si hypoeutectic (Al–7wt.%Si) alloy under the application of electric current with constant parameters flowing through two parallel electrodes into the melt within a cylindrical mold and found that the mechanism of grain refinement driven by electric current is dendrite fragmentation induced by forced flow.

J, Li et al. (Ref 18) have solidified the Al–Si hypereutectic (Al–28.51 wt.%Si) alloy by applying direct electric current and examined the distribution of silicon. Electric current generates a

Semih Birinci, Department of Metallurgical and Materials Engineering, Graduate School of Natural and Applied Sciences, Yıldız Technical University, 34210 İstanbul, Turkey; **Sercan Basit**, Department of Mechanical Engineering, Faculty of Engineering and Architecture, Kırşehir Ahi Evran University, 40100 Kırşehir, Turkey; and **Necmettin Maraşlı**, Department of Mechanical Engineering, Faculty of Engineering, İstanbul Aydın University, Sefaköy-Küçükçekmece, 34294 İstanbul, Turkey. Contact e-mail: necmettinmarasli@aydin.edu.tr.

Joule heat, which slows down the cooling rate and the precipitated area of primary silicon decreases with the increasing the current density. Direct current causes a convection leading to the migration of primary silicon in the opposite direction of electric field, which forms the accumulation area.

Räbiger et al. (Ref 19) have examined the effect of both direct current (DC) and rectangular current pulses (ECP) by applying electric current in their study. After the interaction between the applied current and the self-induced magnetic field, the Lorentz Force is formed, which produces an electro eddy flux and the Lorentz force acts as grain refiner.

The direction of DC electrical current and thus electrical field was normal to the S–L interface growth direction, and the electrical field force acting on the liquid atom does not influence on the atomic mass flux of liquid atoms at the S–L interface in the Al–Si hypoeutectic and Al–Si hypereutectic alloys (Ref 17–19). The magnetic field force and thus Lorentz force affect the atomic mass flux of liquid atoms at the S–L interface. But the magnitudes of applied Lorentz force acting on the liquid Al and Si atoms were not determined or not given for the Al–Si hypoeutectic and Al–Si hypereutectic alloys (Ref 17–19). Joule heating exists in the presence of current in these works (Ref 17–19).

The influences of static external electrical field on the microstructure were clearly seen in the Al–Cu eutectic system, but the researchers could not fully explain the effect of magnitude and direction of external static electrical field on microstructure (Ref 22). The dependence of microstructure parameter on E_+ and E_- was also not identified, and they (Ref 22) have just observed that the E_+ and E_- have affected on the lamellar structure and grain sizes.

More recently, Al–33.0 wt.% Cu and Al–6.4 wt.% Ni, which are well-known eutectic systems, were solidified with different magnitudes of E_+ and E_- (7.0–10.0 kV cm⁻¹) with none current or none joule heating to investigate the influences of E_+ and E_- on λ , HB and σ_{UTS} by Basit et al (Ref 22, 23). They (Ref 22, 23) have observed that lamellar and rod structures, grain sizes and mechanical properties have been significantly influenced by the magnitudes of E_+ and E_- (7.0–10.0 kV cm⁻¹) with none current or none joule heating in the Al–Cu and Al–Ni eutectic systems when the direction of E is same or opposite with the growth direction of S–L interface (Ref 22, 23). According their investigations (Ref 22, 23), the external high DC voltage applied into molten alloy has charged the Al, Cu and Ni atoms as +3 and +2 cations, respectively. Thus, Al⁺³, Cu⁺² and Ni⁺² cations were accelerated by the positive and negative electrical forces, F_+ and F_- , respectively, during the solidification. Therefore, the F_+ and F_- increase and decrease, respectively, the atomic mass flux of liquid Al, Cu and Ni atoms at S–L interface.

The other well-known binary eutectic system is Al–12.6 wt.% Si eutectic system, which has irregular eutectic structure. After the recent work done by Basit et al (Ref 22, 23), the influences of E_+ and E_- on the irregular eutectic microstructure and mechanical properties of Al–Si eutectic alloy were wondered. So how the E_+ and E_- influence on the λ , HB and σ_{UTS} values in the Al–Si eutectic system? It is because the alloying element of Si is semiconductive and the microstructure of Al–Si eutectic system is the irregular eutectic. For this purpose, the Al–Si molten alloy is directionally solidified with different E_+ and E_- values by keeping the existing solidification control parameters at same conditions

and the λ , HB and σ_{UTS} are measured with standard measurement techniques.

2. Materials and Methods

2.1 Experimental Apparatus

An experimental apparatus originally designed by Basit et al (Ref 22) was used to solidify the Al–Si eutectic alloy with different magnitudes of E_+ and E_- in the present work. The details of experimental setup and procedures are given in the literature (Ref 22). The experimental apparatus is schematically illustrated in Fig. 1, and it consists of the external static electrical field system, cooling tank and preheating furnace.

The preheating furnace was build up to prevent immediately solidification of molten alloy into graphite crucible, prepared in the vacuum melting furnace.

20-mm-long cylindrical cooling tank was made of stainless steel, and the water was circulated through to cooling tank to solidify the molten alloy. A 10-mm part of the cooling tank was inserted into hot zone at the bottom of preheating furnace to solidify the molten alloy from bottom to top, and the temperature of cooling tank is kept constant at 291 K using a heating/refrigerating circulator.

An external static electrical field system was set up by connecting the output of FUG HCP 1400-35000 type DC high voltage source terminal to sample and a spacing of 4–6 mm between the sample and the earthed disc as shown in Fig. 2. DC high voltage source supplies the DC voltage up to 35 kV by a maximum 40 mA output current.

The experimental error in the measurements of the space between the sample and stainless steel disc is determined as 2.7% (Ref 22).

2.2 Solidification of the Al–Si Eutectic Alloy Under Static Electrical Field

Al–12.6 wt.% Si eutectic master alloy was prepared by melting the required quantities of Al and Si with 4N and 5N purity of Al and Si, respectively, into a graphite pot (30 mm ID × 40 mm OD and 150 mm in length) under the vacuum. After allowing time to get homogenous melt, the Al–Si molten alloy into the graphite pot was cool down spontaneously under vacuum. Then, the Al–Si master alloy was cut into small pieces and sufficient amount of the Al–Si master alloy was re-melted into another graphite melting crucible (10 mm ID × 40 mm OD, 80 mm in deep and 100 mm long) under vacuum. The molten Al–Si alloy was homogenized by mixing with one end closed an alumina tube with a 25-minute time interval at least 4 times. The preheating furnace was heated up to the melting temperature of alloy while the Al–Si molten alloy was prepared. After homogenization, the graphite pot contains the Al–Si molten alloy, was taken from the vacuum furnace and then placed into the preheated furnace.

The E_+ and E_- were utilized into melts as shown in Fig. 2. The Al–Si molten alloy kept under the high external static electrical field was solidified from bottom to top by turning the cooling water on and the preheating furnace input power off until the preheating furnace temperature was fell down 50 degree below the Al–Si melting temperature. When the melting furnace temperature was 50 degree below the eutectic temperature, the graphite pot was quickly taken out from the

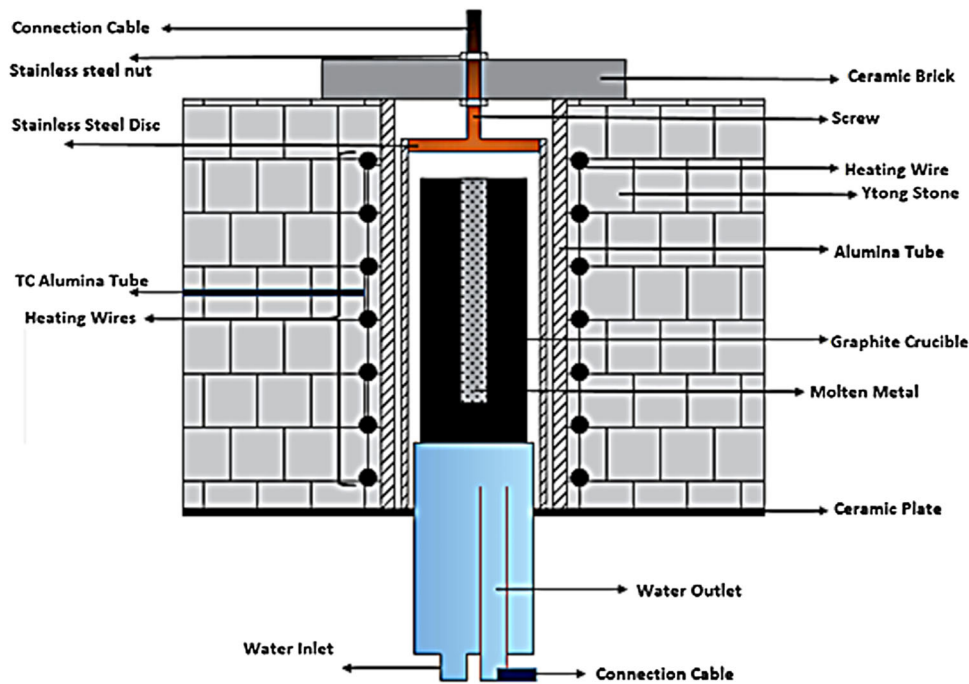


Fig. 1 Schematic representation of experimental apparatus for solidification of alloy under the static electric field

solidification furnace to prevent the heat treatment during the cooling its temperature to room temperature and the graphite pot was broken to remove the specimen. Then, the specimen was rapid quenched into water bath. The solidifications of Al–Si alloy with different E_+ and E_- values (14, 16 and 17.9 kV cm⁻¹) were done. A reference specimen was also solidified without the electric field under existing solidification conditions.

The total experimental error in the determination of E is found be 3.0% (Ref 22, 23).

2.3 Microstructure Observation and Eutectic Spacings Measurements

The solidified sample was 10 mm ID and 80 mm in length. For metallography, 5-mm-thick layer from top of sample was cut out to remove the possible oxide layer, and then, remain part of sample was cut into two pieces of 10 mm in length. After cold mounting of cross sections of these pieces, the sample were grinded and polished by MiniTech263 polishing machine, and then, the specimens were etched with 0.5wt.% HF agent to display the microstructure of the specimens for 35–40s.

The images of microstructures for the Al–Si alloy at near the eutectic composition solidified with different E_+ and E_- magnitudes were photographed with an optical microscope, and the eutectic spacings (λ) were measured from the photographs of microstructure using a software supplied by Nikon Company. At least 10 measurements of λ for each sample were made into a central circle of 5 mm radius for statistical reliability, and then, the average value of λ was considered. The statistical error with standard division in the measurements of λ is about 10% (Ref 23).

2.4 Hardness Measurements

After analyzing of microstructures, the cross-sectional surfaces of specimens were roughly flat by grinding with SiC paper for hardness measurements. The Brinell hardness measurements were made using a BULUT RBOV-200 type hardness tester, which has 62.5 kilograms of load with 2.5 mm in diameter a steel ball. At least 10 HB measurements for each sample were carried out to get reliable hardness value. The estimated experiential error in the hardness measurements is 4% (Ref 23).

2.5 Tensile Test Measurements

10 mm length from each end of samples was cut out, and the remain part of specimens was machined to form a shape, which is shown in Fig. 3 for σ_{UTS} measurements.

The σ_{UTS} values for the Al–Si eutectic alloy solidified with different values of E_+ and E_- were measured by a strain rate of 1mm/min at room temperature using INSTRON 8872 type universal tensile testing machine, which has Bluehill software. The σ_{UTS} measurements were made on longitudinal section of specimen, which is same direction with growth direction of S–L interface, and were repeated at least 4 times. The experimental error in the σ_{UTS} measurements is estimated to be 2% (Ref 23).

3. Results and Discussions

3.1 Influence of the E_+ and E_- on k

Figure 4 shows the microstructures of the Al–Si eutectic alloy solidified with different E_+ and E_- magnitudes. As shown in Fig. 4, the Al–Si eutectic alloy has an irregular eutectic microstructure. It was wonder whether the irregular eutectic

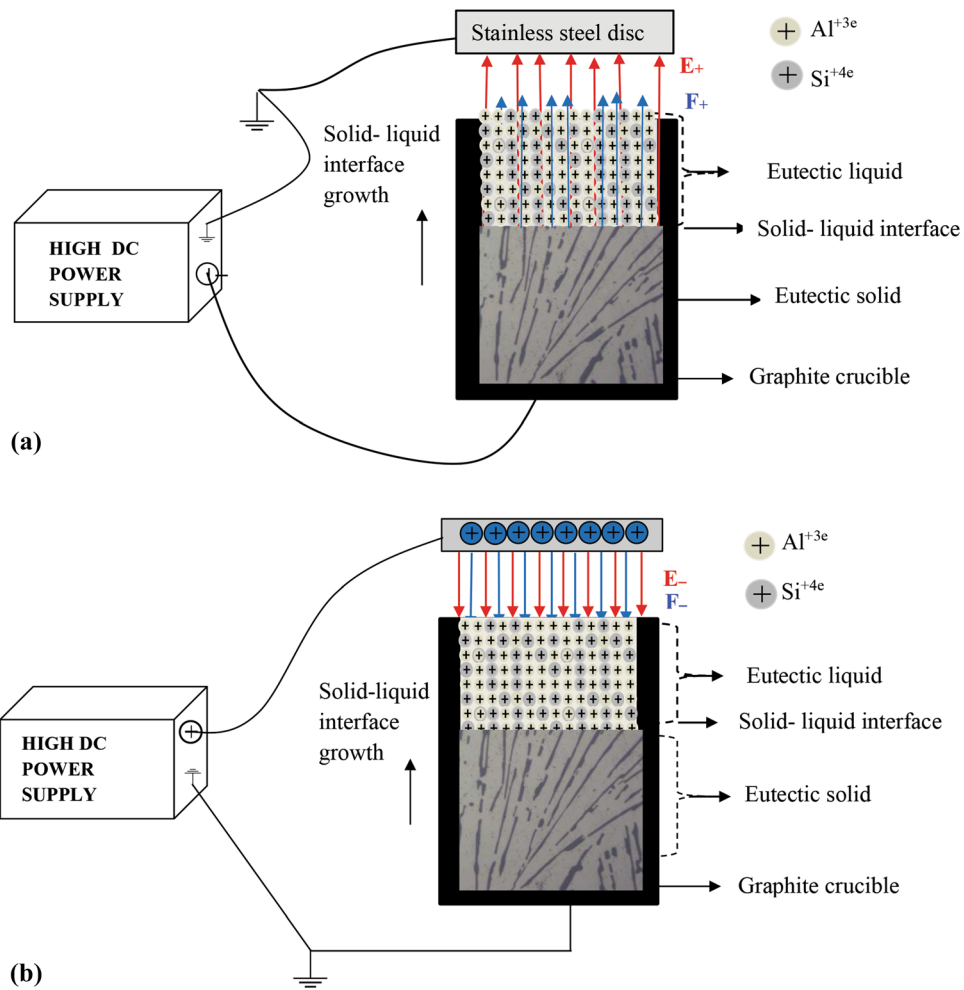


Fig. 2 Schematic illustration of irregular eutectic structure growth under the static electrical field at different directions (a) positive and (b) negative

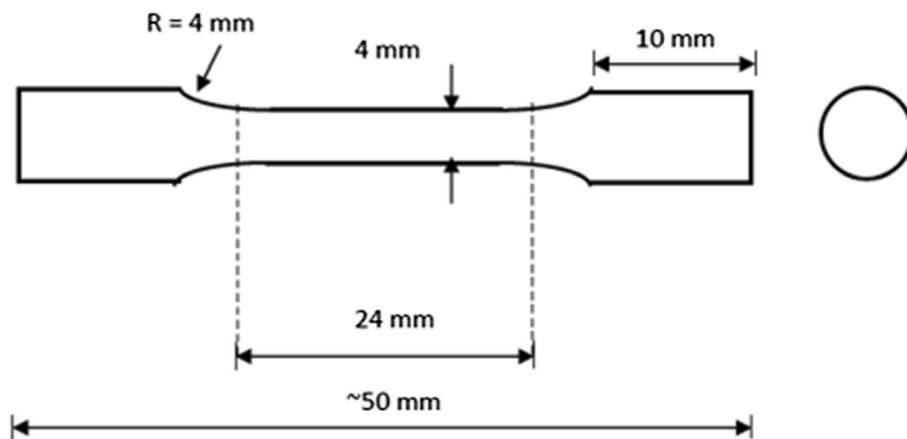


Fig. 3 Geometrical illustration of tensile test specimen

structure could become a regular structure or not with the applied external static electric field?

As shown in Fig. 4, the static external electrical field did not affect the direction of S-L interface growth and the irregularity the Si phase. While E_+ and E_- greatly affected the size of Al matrix phase, it did not affect the Si phase much even though

the E values applied into the Al-Si system are approximately three times the E values applied into the Al-Cu and Al-Ni eutectic systems. Thus, the E_+ and E_- did not affect the λ value in the Al-Si eutectic alloy as much as the λ values in the Al-Cu and Al-Ni eutectic alloys. The atomic mechanism causing these differences can be explained as follows.

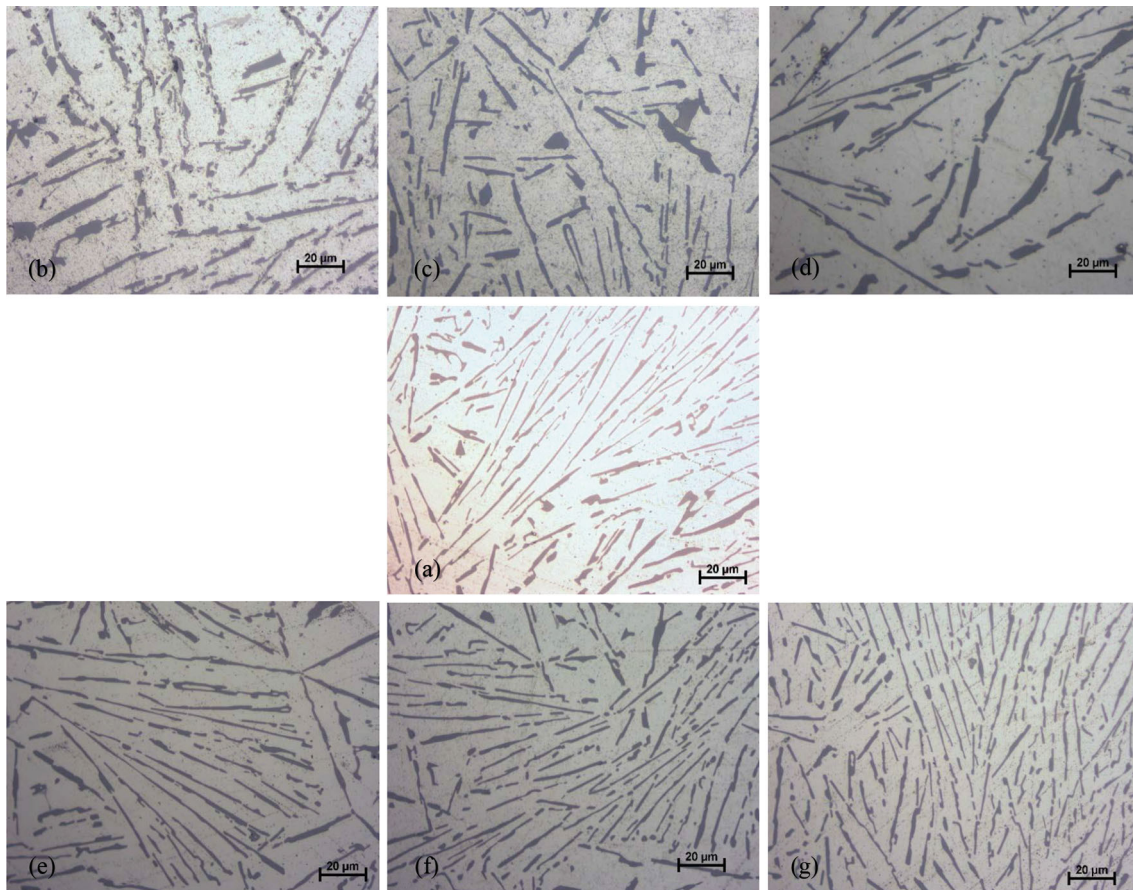


Fig. 4 Optical images of irregular eutectic structure for Al-Si eutectic system solidified with different directions and magnitudes of E ; (a) 0.0 kV cm^{-1} ; (b) 14.0 kV cm^{-1} ; (c) 16.0 kV cm^{-1} ; (d) 17.09 kV cm^{-1} ; (e) -14.0 kV cm^{-1} ; (f) -16.0 kV cm^{-1} ; and (g) $-17.09 \text{ kV cm}^{-1}$

From fundamental of physics, the i specie liquid cation can be accelerated by the F acting on i specie liquid atom, and thus, the acceleration of i specie cation can be expressed as

$$a_i^E = \frac{F_{E,i}}{m_i} = \frac{q_i^* E}{m_i} = \frac{Z_i^* |e| E}{m_i} \quad (\text{Eq 1})$$

where m_i is the atomic mass of i specie ion, $F_{E,i} = q_i^* E$ is the static electrical force acting on i specie cation, $q_i^* = Z_i^* |e|$ is the charge of i specie cation and $E = |\vec{E}|$ is the static electrical field. When the direction of E is parallel or antiparallel to the S-L growth direction, the F_+ and F_- act on each kind of atoms, and thus, the atomic mass flux for each kind of atoms at the S-L interface was influenced by the F_+ and F_- . As can be seen from Eq 1, the magnitude of acceleration for i specie cation depends on Z_i^* and m_i with a constant E . Therefore, the increment or decrement in the V of S-L interface depends on the F_+ and F_- values.

The E_+ and E_- magnitudes were in the range of 14.0 - 17.9 kV cm^{-1} in the present work. As shown in Fig. 4 and Table 1, while the thickness of Al_α phase was enlarged and reduced by increasing the E_+ and E_- values, respectively, the thickness of Si phase was not sufficiently changed by increasing the E_+ and E_- values. It seems that the E_+ and E_- do not strongly affect the irregular structure of Si phase in Al_α matrix. The mechanism of atomic transportation during the solidification under static electrical field might be explained as follows.

Al and Si are metal that will always lose free electrons. The halogens all have seven valence electrons. Each one of these elements wants to gain one electron to achieve an octet. Metals will always lose electrons to form cations. As aluminum has 3 valence electrons, it tends to lose electrons; then, after losing these 3 electrons, it becomes cation, which has +3 charges. Silicon is also a metal, and it can lose its 4 valence electrons and becomes cation, which has +4 charges.

When E_+ and E_- are applied into the Al-Si molten eutectic alloy, it can be assumed that the liquid Al and Si atoms are charged as Al^{+3e} and Si^{+4e} cations, respectively. The magnitudes of F_+ and F_- affecting on Al^{+3e} and Si^{+4e} cations during the solidification must be higher than the sum of surface tension and fraction forces for liquid Al and Si atoms. The present experimental results show that while F_+ and F_- values affecting on liquid Al^{+3e} cation are sufficient to increase or decrease the mass transfer of liquid Al atom, the F_+ and F_- values affecting on liquid Si^{+4e} cation were not sufficient to increase or decrease the mass transfer of liquid Si atom during the solidification.

The critical E value required for changing the size of Al phase in Al-based binary alloy ($E_{critical}^{Al}$) was found as 6 kVcm^{-1} (Ref 22). If liquid Si atom is charged as Si^{+4e} cation with the applied E , the critical value of E required for changing the microstructure of Si phase in Al matrix ($E_{critical}^{Si}$) can be estimated by writing Eq 1 for Al^{+3e} and Si^{+4e} cations and then comparing them into each other to get equal acceleration. The

Table 1 λ , HB and σ_{UTS} values for Al–12.6 wt. pct. Si eutectic system solidified with variable values of E_+ and E_-

| | Static electrical field, E , kV cm^{-1} | | | | | | |
|---|--|-------------|-------------|-------------|-------------|-------------|-------------|
| | -17.9 | -16.0 | -14.0 | 0.0 | 14.0 | 16.0 | 17.9 |
| Average interflake spacings, λ_{Average} (μm) | 3.53±0.8 | 4.18±1.0 | 4.65±0.9 | 5.34±1.1 | 5.37±1.2 | 8.74±2.0 | 10.7±2.8 |
| Average Brinell hardness, HB_{Average} (kg mm^{-2}) | 65.27±2.41 | 63.25±2.53 | 60.23±2.41 | 60.16±2.41 | 58.80±2.35 | 57.83±2.31 | 56.38±2.25 |
| Ultimate tensile stress, σ_{UTS} (N mm^{-2}) | 169.00±3.38 | 165.00±3.30 | 164.00±3.28 | 160.00±3.20 | 157.00±3.14 | 154.00±3.08 | 150.00±3.00 |
| Yield strength (MPa) | 34.31 | 33.61 | 33.18 | 32.29 | 31.50 | 31.39 | 29.23 |
| % Elongation | 2.94 | 2.72 | 2.16 | 1.77 | 2.10 | 2.17 | 2.10 |

accelerations of Al^{+3e} and Si^{+4e} cations should be equal to see similar effects on each Al^{+3e} and Si^{+4e} cations. Therefore, the $E_{\text{critical}}^{\text{Si}}$ value can be estimated from Eq 1 by using the determined value of $E_{\text{critical}}^{\text{Al}}$, and it can be expressed as:

$$E_{\text{critical}}^{\text{Si}} = \frac{q_{\text{Al}} m_{\text{Si}}}{q_{\text{Si}} m_{\text{Al}}} E_{\text{critical}}^{\text{Al}} \quad (\text{Eq 2})$$

The free electrons of Al and Si atoms are +3e and +4e, and the atomic mass of Al and Si atoms is 26.98 and 28.08, respectively. The surface tension of liquid Al and Si is also 0.896 and 0.784 N m^{-1} (Ref [23]), respectively, and they are also close to each other. From Eq 2, the $E_{\text{critical}}^{\text{Si}}$ value is determined to be 5 kV cm^{-1} . The $E_{\text{critical}}^{\text{Si}}$ value of 5 kV cm^{-1} for Si^{+4e} cation is one third of 14.1–17.9 kV cm^{-1} value applied into the Al–Si molten alloy in the present work. Thus, the applied E values (14.1–17.9 kV cm^{-1}) are normally sufficient to increase or decrease the atomic mass flux of Si atoms at the S–L interface if liquid Si atom is charged as Si^{+4e} cation. But the change of Si phase size in the Al matrix by E_+ and E_- was not clearly observed in the present work. From experimental observations, it can be concluded that the liquid Si atom was not charged as Si^{+4e} cation because Si only occurs as ions on the gas phase and only at very high temperatures in a vacuum or inert gas. This means when E_+ and E_- are applied into the Al–Si molten alloy, the liquid Al atom was only charged as Al^{+3e} cation by E_+ and E_- . Thus, the F_+ and F_- affect Al^{+3e} cations and do not affect the uncharged Si atom. The mass transfer of liquid Al atom is affected by F_+ and F_- , and the mass transfer of liquid Si atom is not affected by F_+ and F_- during the solidification of Al–Si molten eutectic alloy under static electrical field. Therefore, the thickness of Al_2 phase is expanding by increasing the value of E_+ or getting thinner by increasing the value of E_- . However, the thickness of Si phase was not considerably changed with increasing the values of E_+ and E_- .

The eutectic spacing (λ) was measured with the triangle method (Ref 24). The λ values were measured from optical images taken from the cross sections of 2 different samples, and the average values of λ are given in Table 1. As shown in Fig. 4 and Table 1, an increment in the average value of λ_{Ave}^+ was observed with increasing E_+ and a decrement in the average value of λ_{Ave}^- was observed with increasing the E_- in the Al–Si eutectic alloy. While the increment in the value of λ_{Ave}^+ is 100% at $E_+ = 17.9 \text{ kV cm}^{-1}$, the decrement in the value of λ_{Ave}^- is 34% at $E_- = 17.9 \text{ kV cm}^{-1}$ in the Al–Si eutectic alloy.

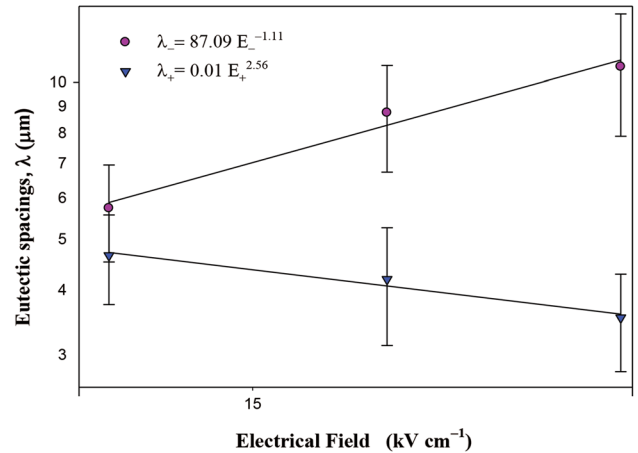


Fig. 5 λ versus E_+ and E_- plots for the Al–Si eutectic system

The average λ versus the E_+ and E_- were plotted in logarithmic scale and are given in Fig. 5. The variation in λ_{Ave} with E_+ and E_- is linear, and the relationships between them were determined from linear regression analysis as

$$\lambda_{\text{Average}}^+(\mu\text{m}) = 0.01 \times E_+^{2.56} \quad (\text{Eq 3})$$

$$\lambda_{\text{Average}}^-(\mu\text{m}) = 87.09 \times E_-^{-1.11} \quad (\text{Eq 4})$$

A comparison of λ dependence on E_+ and E_- for the Al–Si eutectic system obtained in the present work with the λ dependence on V , E_+ and E_- for the Al-based binary or ternary eutectic systems obtained in previous works (Ref 22, 23, 26, 30) is given in Table 2. The exponential 2.56 value of E_+ for Al–Si eutectic system is very close to the exponentials 2.77 and 2.87 values of E_+ for the Al–Cu and Al–Ni eutectic systems (Ref 22, 23), respectively. But the exponential 1.11 value of E_- for Al–Si alloy is 44 and 21% is smaller than the exponentials 2.00 and 1.41 values of E_- for the Al–Cu and Al–Ni eutectic systems (Ref 22, 23), respectively.

The exponential values of E_+ are close to each other for Al–Cu (Ref 22), Al–Ni (Ref 23) and Al–Si eutectic systems. But the exponential 1.4 and 2.0 values of E_- for the Al–Cu and Al–Ni (Ref 22, 23) eutectic systems are bigger than the exponential 1.11 value of E_- for the Al–Si eutectic system. The number of free electrons for Al and Cu, and Ni atoms is 3 and 2, respectively. The free electron number for Cu and Ni atoms is equal, and the atomic mass of Cu and Ni is 63.5 and 58.69,

Table 2 A comparison of λ , HB and σ_{UTS} dependences on E_+ and E_- for Al–12.6 wt. pct

| Alloy, wt. % | Solidification parameters | | | Static electrical field, kVcm ⁻¹ |
|--|--|--|---|---|
| | G, K/mm | V, $\mu\text{m/s}$ | | |
| Al–12.6Si (present study) | ... | ... | | From 14 to 17.9 |
| Al–33.0Cu (Ref 20) | ... | ... | | From 8.1 to 10 From –8 to –10.2 |
| Al–6.4Ni (Ref 21) | ... | ... | | From 8 to 10 From –7.8 to–10.2 |
| Al–12.6Si (Ref 22) | 7.8 | 8.3–498.7 | | ... |
| Al–13Si (Ref 24) | 7–14 | 10–2000 | | ... |
| Al–12.95Si–4.96Mg (Ref 25) | 9.39 | 8.64–165.20 | | ... |
| Al–12Si–5Ni–0.4Fe (Ref 26) | 6.43 | 8.25–164.81 | | ... |
| Alloy, wt. % | Eutectic spacings, μm | Hardness, kg mm ⁻² | Ultimate tensile strength, N mm ⁻² | |
| Al–12.6Si (present study) | $\lambda^+ = 0.01 \times E_+^{2.56}$ $\lambda^- = 87.09 \times E_-^{-1.11}$ | $HB^+ = 91.20 \times E_+^{-0.16}$ $HB^- = 25.11 \times E_-^{0.32}$ | $\sigma_{UTS}^+ = 251.18 \times E_+^{-0.18}$ | $\sigma_{UTS}^- = 125.89 \times E_-^{0.09}$ |
| Al–33.0Cu (Ref 20) | $\lambda^+ = 1.672 \times E_+^{2.77}$ $\lambda^- = 0.482 \times E_-^{-2.00}$ | $HB^+ = 103.83 \times E_+^{-0.96}$ $HB^- = 5.51 \times E_-^{0.51}$ | $\sigma_{UTS}^+ = 220.29 \times E_+^{-0.77}$ | $\sigma_{UTS}^- = 308.81 \times E_-^{0.45}$ |
| Al–6.4Ni (Ref 21) | $\lambda^+ = 2.57 \times E_+^{2.87}$ $\lambda^- = 0.73 \times E_-^{-1.41}$ | $HB^+ = 2102.03 \times E_+^{-0.61}$ $HB^- = 0.602 \times E_-^{0.63}$ | $\sigma_{UTS}^+ = 111.99 \times E_+^{1.31}$ | $\sigma_{UTS}^- = 256.79 \times E_-^{1.12}$ |
| Al–12.6Si (Ref 22) | $\lambda = 23.44 \times V^{-0.46}$ | ... | ... | ... |
| Al–13Si (Ref 24) | $\lambda = 55.0 \times V^{-0.52}$ | ... | ... | ... |
| Al–12.95Si–4.96Mg (Ref 25) | $\lambda = 29.32 \times V^{-0.52}$ | $HV = 119.9 \times V^{0.07}$ | $\sigma_{UTS} = 222.84 \times V^{0.20}$ | |
| Al–12Si–5Ni–0.4Fe (Ref 26) | $\lambda = 9.94 \times V^{-0.38}$ | $HV = 67.9 \times V^{0.07}$ | $\sigma_{UTS} = 177.86 \times V^{0.11}$ | |
| Si eutectic system obtained in present work with λ , HB and σ_{UTS} dependences on V , E_+ and E_- for the Al-based binary or ternary alloys obtained in previous works | | | | |

respectively. The free electron number for Al atom is 30% higher than the free electron numbers for Cu and Ni atoms, but the atomic mass of Al is one third of atomic mass of Cu and Ni. According to the results obtained for the Al–Si eutectic system, Si liquid atom which was not charged with E_+ and E_- or the F_+ and F_- affecting Si^{+4} liquid ion is not sufficient high to increase or decrease the atomic mass transfer of liquid Si atom at the S–L interface. The eutectic melting temperature of Al–Cu, Al–Si and Al–Ni systems is 821, 850 and 913 K, respectively. Therefore, the atomic mass flux due to the E_+ and E_- at the S–L interface is very complicate and depends on free electron numbers and atomic mass, alloy composition and melting temperature during the solidification.

Table 2 also shows the λ dependence on E_+ is 4 times of the λ dependence on V and the λ dependence on E_- is at least twice of the λ dependence on V in Al–Si binary or ternary alloys. The influences of E_+ and E_- on λ are higher than the influence of V on λ , and thus, the both magnitude and direction of E are an external control parameter for solidification when its direction is parallel or antiparallel to the S–L interface growth direction.

3.2 Dependence of HB on E_+ and E_-

The Brinell hardness measurements for the Al–Si alloy were made on the cross sections of samples, which are directionally solidified with different E_+ and E_- , and the average Brinell hardness (HB) values are given in Table 1. As mentioned above, λ_{Ave}^+ increases, and thus, the HB^+ decreases with increasing the value of E_+ , but the λ_{Ave}^- decreases and the HB^- increases with increasing the value of E_- . These decreases or increases in the HB values due to the changing of the Al phase size with E_+ and E_- are theoretically expected variations. The variations in HB with E are plotted in Fig. 6, and the relationships between them are found as:

$$HB^+ = 91.20 \times E_+^{-0.16} \quad (\text{Eq 5})$$

$$HB^- = 25.11 \times E_-^{0.32} \quad (\text{Eq 6})$$

As shown in Table 1 and Fig. 6, the applied external static electric E_+ and E_- into the Al–Si molten alloy during the solidification seems to clearly influence the HB as well as the λ . The HB^+ values for the sample solidified at 14.0, 16.0 and 17.9 $kV\ cm^{-1}$ were measured to be 60.23, 63.25 and 65.27 $kg\ mm^{-2}$,

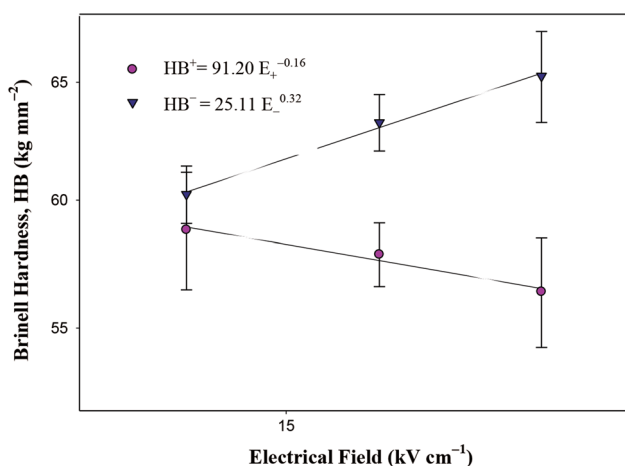


Fig. 6 HB versus E_+ and E_- plots for the Al–Si eutectic system

respectively, while the HB^- values for the samples solidified at -14.0 , -16.0 and $-17.9\ kV\ cm^{-1}$ were also measured as 58.79, 57.82 and 56.7 $kg\ mm^{-2}$, respectively. The HB^+ and HB^- values measured in the present work are the average value of 10 hardness measurements for each sample.

The exponential 0.16 value of E_+ is about half of exponential 0.32 value of E_- in the Al–Si. This means that the E_- is more effective than the E_+ in the Al–Si eutectic system.

The HB^+ and HB^- dependences on E_+ and E_- for the Al–Si eutectic system determined in the present work were also compared with the HB dependences on V , E_+ and E_- for the Al-based binary and ternary eutectic systems determined in previous works (Ref 22, 23, 26, 30) and are given in Table 2. Exponential 0.16 value of E_+ for the Al–Si eutectic system is about one fourth and one sixth of exponential 0.61 and 0.96 values of E_+ for Al–Ni (Ref 23) and Al–Cu (Ref 22) eutectic systems, respectively. The exponential 0.32 value of E_- for the Al–Si eutectic system is about half of the exponentials 0.63 and 0.51 values of E_- for Al–Ni (Ref 23) and Al–Cu (Ref 22), respectively.

Additionally, Table 2 shows that HB dependence on E_+ and E_- is stronger than the HB dependence on V in the Al–Si binary and multicomponent systems.

4. Effects of E_+ and E_- on r_{UTS}

Figure 7 shows the ultimate tensile stress versus strain curves for the Al–Si eutectic alloy directionally solidified with different E_+ and E_- values. The σ_{UTS} , YS and %El values for the Al–Si eutectic alloy were determined from stress–strain graphs and are given in Table 1.

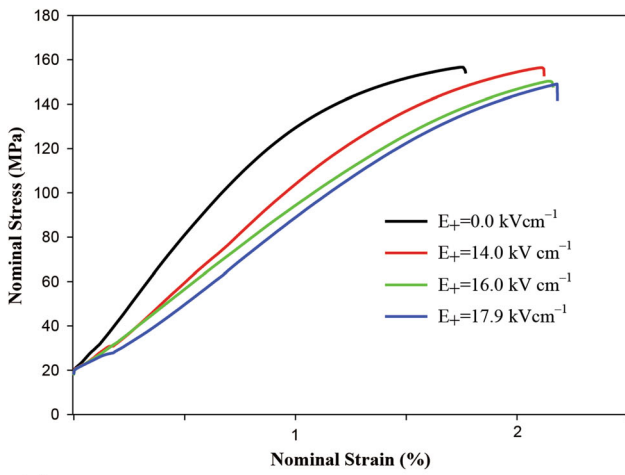
Figure 8 shows the variations in σ_{UTS} with E_+ and E_- . Figure 8 and Table 1 show the σ_{UTS} value decreases with increasing E_+ while the σ_{UTS} value increases with increasing E_- . The reason for this difference is the exactly same reason with hardness variations. Again, the E_+ and E_- affected the atomic mass flux of liquid Al atoms at the S–L interface during the solidification and the growth rate of S–L interface increases or decreases. Thus, any increment or decrement in the V value due to E_+ and E_- affects the microstructure and thus the mechanical properties of alloys.

The relationships between σ_{UTS} and E_+ and E_- were determined with regression analysis as:

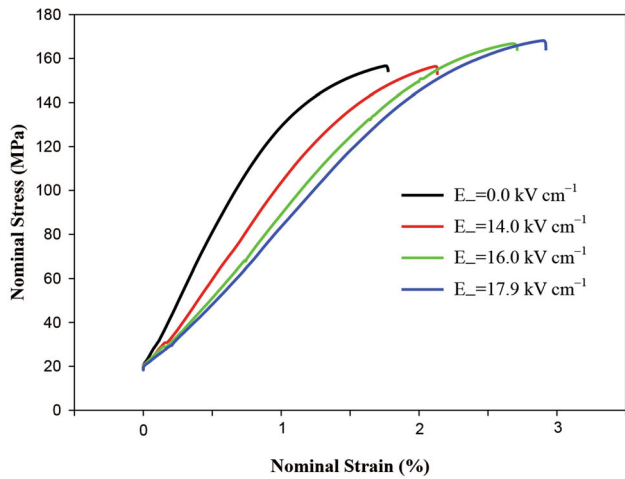
$$\sigma_{UTS}^+ = 251.18 \times E_+^{-0.18} \quad (\text{Eq 7})$$

$$\sigma_{UTS}^- = 125.89 \times E_-^{0.09} \quad (\text{Eq 8})$$

The influences of E_+ and E_- on σ_{UTS} for the Al–Si irregular system are compared with the influences of E_+ , E_- and V on σ_{UTS} for the Al-based binary or ternary alloys obtained in previous works (Ref 22–26) and given in Table 2. The exponential 0.18 and 0.09 values of E_+ and E_- , respectively, for the Al–Si irregular eutectic system are very close to the exponential 0.20 and 0.11 values of V for the Al–Si–Mg (Ref 26) and Al–Si–Ni–Fe (Ref 27) irregular eutectic system, respectively. The exponential 0.18 value of E_+ for the Al–Si irregular eutectic system is one fourth and one sixth of exponentials 0.77 and 1.31 values of E_+ for Al–Cu (Ref 22) and Al–Ni (Ref 23) eutectic systems, respectively. Neverthe-



(a)



(b)

Fig. 7 Stress-strain curves for the Al-Si eutectic system solidified with different values of (a) E_+ and (b) E_-

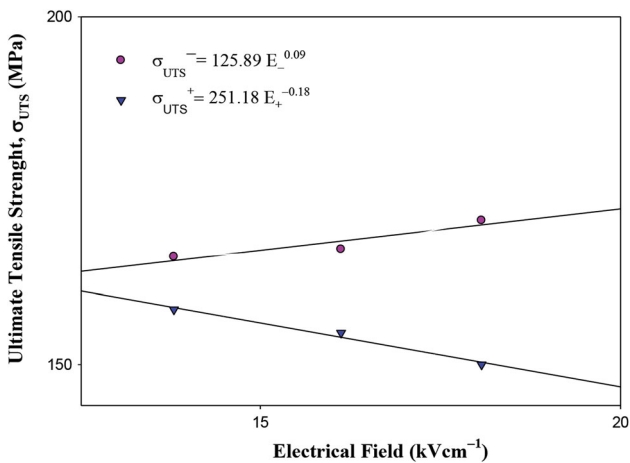


Fig. 8 σ_{UTS} versus E_+ and E_- plots for the Al-Si eutectic system

less, the exponential 0.09 value of E_- for the Al-Si irregular eutectic system is one fifth and one tenth of exponentials 0.45 and 1.12 values of E_+ for the Al-Cu (Ref 22) and Al-Ni (Ref

23) eutectic systems, respectively. From Table 2, it can be also concluded that the dependences of σ_{UTS} on E_+ and E_- for the Al-Si irregular eutectic system are not stronger than the dependence of σ_{UTS} on E_+ and E_- for the Al-Cu (Ref 22) and Al-Ni (Ref 23) regular eutectic systems.

As shown in Table 1, the YS and %El for the Al-Si eutectic alloy are also affected from E_+ and E_- . Increment in the YS value is about 6% with increasing E_- while decrement in the YS value is about 10%. According to %El values shown in Table 1, the %El value increases about 4% and 2% by increasing E_- and E_+ values, respectively. It is expected that when the YS value increases, the %El value should be decreased or vice versa. But the %El also increased while YS value increased by increasing E_+ value in the present work. This disparity might be coming from an error in the determination of %El value.

From the above discussion, it might be expressed that the microstructure and physical and mechanical properties for alloys produced by electrically chargeable metals can be controlled by the external control parameter of static E when its direction is parallel or antiparallel to the S-L growth direction.

5. Conclusions

Both the direction and magnitude of E applied into Al-Si molten alloy did not affect the S-L interface growth direction and the irregularity Si phase. While E_+ and E_- affect effectively the size of Al matrix phase, the size of Si phase was not affected by E_+ and E_- because liquid Si atom was not charged with the E_+ and E_- . The F_+ and F_- acting on charged liquid Al atoms increase or decrease the acceleration of the liquid Al atoms at the S-L interface during the transformation from liquid to solid. Therefore, the F_+ and F_- lead an increment or decrement in the atomic mass flux of liquid Al atoms at the S-L interface when its direction is parallel or antiparallel to the S-L interface growth direction. Thus, the λ , HB and σ_{UTS} values in the Al-Si eutectic system are not affected as much as in the Al-Cu and Al-Ni eutectic systems by E_+ and E_- magnitudes. Therefore, dependence of λ , HB and σ_{UTS} on E_+ and E_- in the Al-Cu and Al-Ni eutectic alloys are stronger than dependence of λ , HB and σ_{UTS} on E_+ and E_- in the Al-Si eutectic alloy.

From experimental results, it can be concluded that the external static E plays an affective role to control the atomic mass flux for alloys at the S-L interface during the solidification of alloys produced by electrically chargeable metals when its direction is parallel or antiparallel with S-L interface growth direction.

Acknowledgments

This work was supported by the Scientific and Technical Research Council of Turkey (TUBİTAK-118M695) and Yıldız Technical University Scientific Research Project Unit (FBA-2017-3078). The tensile test measurements were done by Çelik Halat ve Tel Sanayi A.Ş. The authors are grateful to the Scientific and Technical Research Council of Turkey (TUBİTAK-118M695) and Yıldız Technical University Scientific Research Project Unit (FBA-2017-3078) for their financial supports and Çelik Halat ve Tel

Sanayi A.Ş. Company for their help to the tensile test measurements.

Conflict of interest

The authors declare that they have no conflict of interest.

References

1. S.G. Shabestari and H. Moemeni, Effect of Copper and Solidification Conditions on the Microstructure and Mechanical Properties of Al-Si-Mg Alloys, *J. Mater. Process. Technol.*, 2004, **153–154**, p 193–198
2. A.K. Dahle, K. Nogita, S.D. McDonald, C. Dinnis and L. Lu, Eutectic Modification and Microstructure Development in Al-Si Alloys, *Mater. Sci. Eng. A.*, 2005, **413–414**, p 243–248
3. S.S. Sreeja Kumari, R.M. Pillai, T.P.D. Rajan and B.C. Pai, Effects of Individual and Combined Additions of Be, Mn, Ca and Sr on the Solidification Behaviour, Structure and Mechanical Properties of Al-7Si-0.3Mg-0.5Fe Alloy, *Mater. Sci. Eng. A.*, 2007, **460–461**, p 561–573
4. J.E. Gruzleski and B.M. Closset, *The Treatment of Liquid Aluminum-Silicon Alloys*, Am. Foundrymen's Soc, USA, 1990
5. C. Brian and K. O'Reilly, *Solidification and Casting*, Insitute of Physics Publisng Bristol and Philadelphia, United Kingdom, 2003
6. E. Sjölander and S. Seifeddine, The Heat Treatment of Al-Si-Cu-Mg Casting Alloys, *J. Mater. Process. Technol.*, 2010, **210**, p 1249–1259. (English)
7. S. Hegde and K.N. Prabhu, Modification of Eutectic Silicon in Al-Si Alloys, *J. Mater. Sci.*, 2008, **43**, p 3009–3027
8. R. Li, L. Liu, L. Zhang, J. Sun, Y. Shi and B. Yu, Effect of Squeeze Casting on Microstructure and Mechanical Properties of Hypereutectic Al-xSi Alloys, *J. Mater. Sci. Technol.*, 2017, **33**, p 404–410
9. A. Kisasoz, K.A. Guler and A. Karaaslan, Influence of Orbital Shaking on Microstructure and Mechanical Proeperties of A380 Aluminum Alloy Produced by Lost Foam Castin, *Russ. J. Non-Ferrous Met.*, 2017, **58**, p 238–243
10. H.K. Jung and C.G. Kang, Induction Heating Process of an Al-Si Aluminum Alloy, *J. Mater. Process. Technol.*, 2002, **120**, p 355–364
11. Q.D. Qin, Y.G. Zhao, P.J. Cong, W. Zhou and B. Xu, Semisolid Microstructure of Mg₂Si/Al Composite by Cooling Slope Cast and its Evolution During Partial Remelting Process, *Mater. Sci. Eng. A.*, 2007, **444**, p 99–103
12. H. Conrad, Influence of an Electric or Magnetic Field on the Liquid-Solid Transformation in Materials and on the Microstructure of the Solid, *Mater. Sci. Eng. A.*, 2000, **287**, p 205–212
13. Y. Zhong, J. Wang, T. Zheng, Y. Fautrelle and Z. Ren, Homogeneous Hypermonotectic Alloy Fabricated by Electric-Magnetic-Compound Field Assisting Solidification, *Mater. Today: Proc.*, 2015, **2**, p 364–372
14. Z.Y. Liao, H.C. Wang, P. Hong, X. Li, J. Lie, S.J. Wang, G. Wang and M.S. Dargusch, Effect of Pulsed Electric Field on the Distribution and Migration of P S, and Si Elements of Fe- Based Alloys, *Adv. Mater. Res.*, 2011, **194–196**, p 371–434
15. Y. Ma, L.L. Zheng and D.J. Larson, Microstructure Formation During BiMn/Bi Eutectic Growth with Applied Alternating Electric Fields, *J. Cryst. Growth*, 2004, **262**, p 620–630
16. T. Manuwong, *Solidification of metal alloys in pulse electromagnetic fields* (Ph.D Thesis, University of Hull, UK, 2015)
17. Y.H. Zhang, Y.Y. Xu, C. Y. Ye, C. Sheng, J. Sun, G. Wang, X.C. Miao, C.J. Song and Q.J. Zhai, Relevance of electrical current distribution to the forced flow and grain refinement in solidified Al-Si hypo eutectic alloy, *Scientific Reports*, 2018, **8**, 3242
18. J. Lia, P. Ni and L. Wang, Tan Influence of Direct Electric Current on Solidification Process of Al-Si Alloy, *Mater. Sci. Semiconductor Process.*, 2017, **61**, p 79–84
19. D. Rübiger, Y. Zhang, V. Galindo, S. Franke, B. Willers and S. Eckert, Experimental Study on Directional Solidification of Al-Si Alloys Under the Influence of Electric Currents, *Mater. Sci. Eng.*, 2016, **143**, p 12–21
20. K.G. Prashanth, S. Scudino, H.J. Klaus, K.B. Surreddi, L. Löber, Z. Wang, A.K. Chaubey, U. Kühn and J. Eckert, Microstructure and Mechanical Properties of Al-12Si Produced by Selective Laser Melting: Effect of Heat Treatment, *Mater. Sci. Eng. A.*, 2014, **590**, p 153–160
21. B. Liu, Z. Zhao, Y. Wang and Z. Chen, The Solidification of Al-Cu Binary Eutectic Alloy with Electric Fields, *J. Cryst. Growth*, 2004, **271**, p 294–301
22. S. Basit, S. Birinci and N. Maraşlı, Electro Growth of Al-Cu Eutectic Alloy, *Mater. Charact.*, 2020, **161**, p 110157
23. S. Basit, S. Birinci and N. Maraşlı, Growth of Rod Structure with Static Electrical Field in the Al-Ni Eutectic System, *J. Mater. Sci. Mater. Electron.*, 2020, **31**, p 14055–14068
24. M. Gündüz, H. Kaya, E. Çadırli and A. Özmen, Eutectic Spacing and Undercoolings in Al-Si Irregular Eutectic Alloy, *Mater. Sci. Eng. A.*, 2004, **369**, p 215–229
25. I. Egry, E. Ricci, R. Novakovic and S. Ozawa, Surface Tension of Liquid Metals and Alloys-Recent developments, *Adv. Coll. Interface. Sci.*, 2010, **159**, p 198–212
26. S. Steinbach, N. Euskirchen, V. Witusiewicz, L. Sturz and L. Ratke, The Influence of Fluid Flow on Intermetallic Phases in Al-Cast Alloys, *Mater. Sci. Forum*, 2006, **519–521**, p 1795–1800
27. N. El Mahallawy, A. Fathy, W. Abdelaziem and M. Hassan, Microstructure Evolution and Mechanical Properties of Al/Al-12%Si Multilayer Processed by Accumulative Roll Bonding (ARB), *Mater. Sci. Eng. A.*, 2015, **647**, p 127–135
28. T. Hosch and R.E. Napolitano, The Effect of the Flake to Fiber Transition in Silicon Morphology on the Tensile Properties of Al-Si Eutectic Alloys, *Mater. Sci. Eng. A.*, 2010, **528**, p 226–232
29. Y. Kaygisiz and N. Maraşlı, Microstructural, Mechanical and Electrical Characterization of Directionally Solidified Al-Si-Mg Eutectic Alloy, *J. Alloys Compd.*, 2015, **618**, p 197–203
30. E. Çadırli, U. Büyük, S. Engin and H. Kaya, Effect of Silicon Content on Microstructure, Mechanical and Electrical Properties of the Directionally Solidified Al-Based Quaternary Alloys, *J. Alloys Compd.*, 2017, **694**, p 471–479

Publisher's Note Springer Nature remains neutral with regard to jurisdictional claims in published maps and institutional affiliations.